Pre-Steady-State and Steady-State Kinetic Analysis of *E. coli* Class I Ribonucleotide Reductase†

Jie Ge,‡ Guixue Yu,‡,§ Mark A. Ator,‡,|| and JoAnne Stubbe*,‡,⊥

Department of Chemistry and Biology, Massachusetts Institute of Technology, Cambridge, Massachusetts 02139

Received March 13, 2003; Revised Manuscript Received May 21, 2003

ABSTRACT: *E. coli* ribonucleotide reductase (RNR) catalyzes the conversion of nucleoside diphosphates (NDPs) to dNDPs and is composed of two homodimeric subunits: R1 and R2. R1 binds NDPs and contains binding sites for allosteric effectors that control substrate specificity and turnover rate. R2 contains a diiron-tyrosyl radical (Y•) cofactor that initiates nucleotide reduction. Pre-steady-state experiments with wild type R1 or C754S/C759S−R1 and R2 were carried out to determine which step(s) are rate-limiting and whether both active sites of R1 can catalyze nucleotide reduction. Rapid chemical quench experiments monitoring dCDP formation gave k_{obs} of 9 ± 4 s^{-1} with an amplitude of 1.7 ± 0.4 equiv. This amplitude, generated in experiments with pre-reduced R1 (3 or 15 μM) in the absence of reductant, indicates that both monomers of R1 are active. Stopped-flow UV−vis spectroscopy monitoring the concentration of the Y• failed to reveal any changes from 2 ms to seconds under similar conditions. These pre-steady-state experiments, in conjunction with the steady-state turnover numbers for dCDP formation of 2−14 s^{-1} at RNR concentrations of 0.05−0.4 μM (typical assay conditions), reveal that the rate-determining step is a physical step prior to rapid nucleotide reduction and rapid tyrosine reoxidation to Y•. Steady-state experiments conducted at RNR concentrations of 3 and 15 μM, typical of pre-steady-state conditions, suggest that, in addition to the slow conformational change(s) prior to chemistry, re-reduction of the active site disulfide to dithiol or a conformational change accompanying this process can also be rate-limiting.

Ribonucleotide reductases catalyze the reduction of ribonucleotides to deoxyribonucleotides (Scheme 1), essential building blocks required for DNA replication and repair (*1*−*3*). RNRs[1] have been divided into three classes based on the metallo-cofactors that generate a thiyl radical (S•) in structurally homologous active sites (*4*−*6*). Each class uses different

Scheme 1

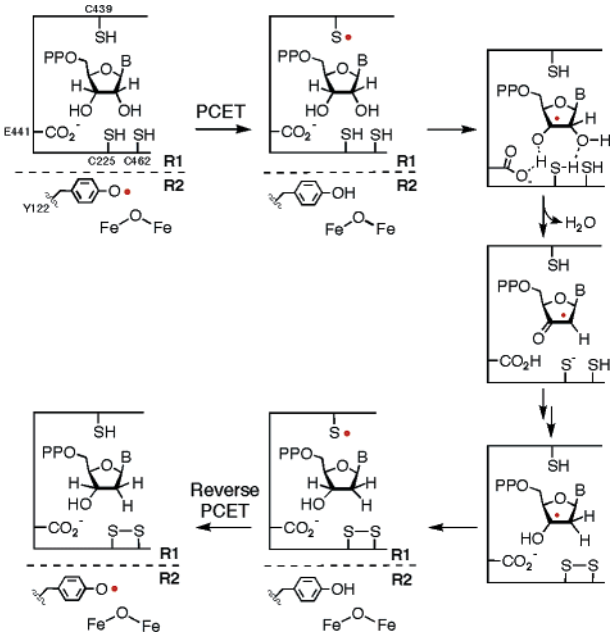

radical initiators. The class I RNRs use a diferric-tyrosyl radical (Y•) cofactor. The class II RNRs use adenosylcobalamin (AdoCbl), and the class III RNRs use a glycyl radical, generated by a process that requires an [Fe−S] cluster and S-adenosyl methionine. The mechanism of nucleotide reduction of the class I and II RNRs has been studied extensively (Scheme 1) (*1*). In contrast to the class II RNRs (*7*−*12*), the

† This work was supported by NIH Grant #GM29595.

* Corresponding author. Address: Department of Chemistry, Building 18-Room 598, Massachusetts Institute of Technology, 77 Mass. Ave, Cambridge, MA 02139. Phone: 617 2531814. Fax: 617 2587247. E-mail: stubbe@mit.edu.

‡ Department of Chemistry.

§ Present Address: Discovery Chemistry, Hopewell Site, Bristol-Myers Squibb, Princeton, NJ 08543.

|| Present Address: Department of Biochemistry, Cephalon, Inc., West Chester, PA 19380.

⊥ Department of Biology.

[1] Abbreviations: AdoCbl, 5′-deoxyadenosylcobalamin; ADP, adenosine 5′-diphosphate; ATP, adenosine 5′-triphosphate; CDP, cytidine 5′-diphosphate; dADP, 2′-deoxyadenosine 5′-diphosphate; dATP, 2′-deoxyadenosine 5′-triphosphate; dC, deoxycytidine; dCDP, 2′-deoxycytidine 5′-diphosphate; dCK, deoxycytidine kinase; dGTP, 2′-deoxyguanosine 5′-triphosphate; dNDP, deoxynucleoside 5′-diphosphate; dNTP, deoxynucleoside 5′-triphosphate; DTT, 1,4-dithiothreitol; equiv, equivalents; EDTA, ethylenediaminetetraacetic acid; EPR, electron paramagnetic resonance spectroscopy; HEPES, *N*-(2-hydroxyethyl)-piperazine-*N*′-(2-ethanesulfonic acid); NADPH, reduced β-nicotinamide adenine dinucleotide phosphate; NDP, nucleoside diphosphate; PCET, proton-coupled electron transfer; RNR, ribonucleotide reductase(s); RTPR, the *L. leichmannii* class II RNR; S•, thiyl radical; SA, specific activity; SF, stopped-flow; TEAB, triethylammonium bicarbonate; TR, thioredoxin; TRR, thioredoxin reductase; TTP, thymidine 5′-triphosphate; UDP, uridine 5′-diphosphate; wt, wild type; Y•, tyrosyl radical; 1 U, is one nmol/min.

10.1021/bi034374r CCC: $25.00
Published on Web 08/05/2003

rate-limiting step or steps in the catalysis of the class I enzymes have yet to be identified. Steady state and pre-steady-state experiments have been undertaken and are now presented in an effort to elucidate unresolved kinetic issues. Defining the rate-limiting step(s) in the class I RNR from *Escherichia coli* is essential in designing experiments that elucidate the mechanism of radical initiation in these enzymes.

The *E. coli* class I RNR is composed of two homodimeric subunits: R1 and R2. The active form of the protein is proposed to be a 1:1 complex of these subunits (*13*, *14*). Nucleoside diphosphate (NDP) reduction takes place on the large subunit R1, which contains five conserved, essential cysteines per monomer (*15*−*20*). R1 also contains at least two, and possibly three, types of allosteric effector binding sites that regulate enzyme activity and substrate specificity (*21*−*24*). R2 contains a stable and essential Y• radical (residue 122), which is adjacent to a μ-oxo bridged diferric cluster. R2 as isolated contains 0.9−1.3 Y•s per dimer. The unusual stoichiometry of Y• per R2 raises issues as to whether both monomers of dimeric R1 are catalytically active. During catalysis, Y122• on R2 is thought to function as a radical chain initiator by generating a S• on C439 of R1 via a proposed long-range proton-coupled electron transfer (PCET) pathway (*25*, *26*). The S• of C439 in turn is proposed to abstract the 3′ hydrogen atom from substrate NDP and initiate nucleotide reduction chemistry (Scheme 1) (*19*). Two R1 active site cysteines, C225 and C462, provide the reducing equivalents by forming a disulfide bond concomitant with deoxynucleotide formation (*15*−*18*). Two additional cysteines located at the C-terminus of R1, C754 and C759 (not shown in Scheme 1), are required for the reduction of active site disulfide by thioredoxin (TR) or glutaredoxin (*18*). The structures of R1 determined crystallographically reveal that the C-terminus of R1 (the last 24 amino acids) is thermally labile (*6*, *25*), leaving open the question of the mechanism by which this tail, containing C754 and C759, interacts with the active site to re-reduce the C225−C462 disulfide and with thioredoxin to reduce the C754−C759 disulfide. Structures of R2 are also available (*27*, *28*). There is, however, no structure of any R1R2 complex, which leaves the mechanism of radical initiation by the Y• of R2 unresolved. A docking model based on shape complementarity between R1 and R2 and extensive biochemical data suggests that Y122• of R2 is located 35 Å away from C439 of R1 (*25*). Understanding the basis for this radical initiation requires an understanding of R1−R2 interactions and which step or steps limit nucleotide reduction.

While our work was in progress, Erickson reported the first pre-steady-state experiments to investigate the kinetic mechanism of *E. coli* RNR (*29*, *30*). Polyclonal antibodies were generated that recognized peptides containing C225 and the peripheral cysteines (C754 and C759). The antibodies were used to analyze rapid chemical quench samples for the rate of formation of the active site and peripheral disulfides. These studies led to the model summarized in Scheme 2A. This model requires that only one of the two monomers of R1 is active and that the active site cysteines of one monomer that become oxidized during dCDP formation can be re-reduced by the peripheral cysteines on either of the R1 monomers. The model further predicts that 3 equiv of dCDP are produced in a single-exponential phase and that both

Scheme 2

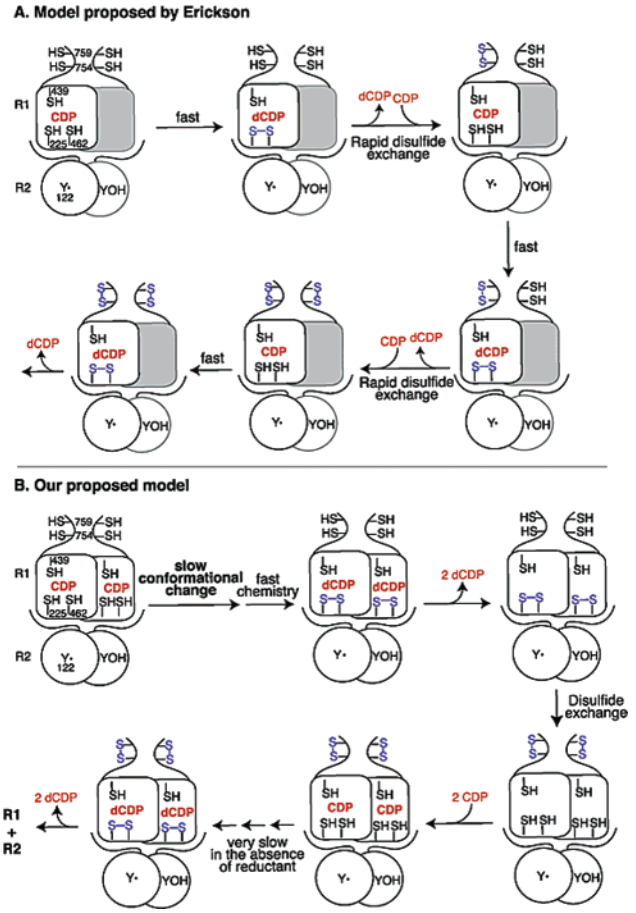

intramolecular and intermolecular disulfide interchanges between the C-terminal cysteines and the active site cysteines are rapid relative to the rate of dCDP formation.

To determine which step or steps are rate-limiting and whether the active site in each monomer of R1 is active, we have carried out steady-state and pre-steady-state studies in which dCDP formation has been monitored by rapid chemical quench experiments and the changes in the Y• have been monitored by stopped-flow (SF) UV−vis spectroscopy. These studies suggest a model that differs substantially from that of Erickson (Scheme 2B). Evidence is presented on the basis of experiments with wild type (wt) R1 and the C754S/C759S double mutant of R1, which suggest that both monomers of R1 are active and that, while disulfide interchange between the active site cysteines and the peripheral cysteines may occur rapidly, only two dCDPs are produced in a kinetically competent fashion in the absence of external reductants. Additional studies are presented that suggest that the rate determining step in the class I RNR is a physical step gating long-range radical initiation between R2 and R1, and/or re-reduction of the active site disulfide. Finally, our studies suggest that the Y• of R2 is reduced and oxidized on each turnover.

MATERIALS AND METHODS

Materials. [2-^{14}C]-Cytidine (250 μCi, 55 mCi/mmol, 99.2% pure) was purchased from Moravek Biochemicals (MC128, lot #146-229-055). Triethylamine (99% pure) was available from Acros. *N*-(2-Hydroxyethyl)piperazine-*N*′-(2-

ethanesulfonic acid) (HEPES) was purchased from US Biochemicals. 1,4-Dithiothreitol (DTT) was purchased from Mallinckrodt. DEAE Sephadex A-25 was purchased from Pharmacia. Boronate Affi-Gel 601 and Dowex AG 1 × 8 were purchased from Bio-Rad. Myokinase [M3003, specific activity (SA) = 1750 U/mg], cytidine, ATP, dATP, CDP, β-NADPH, EDTA, hydroxyurea, and other chemicals were purchased from Sigma. Calf intestine alkaline phosphatase was purchased from Roche. *E. coli* TR was isolated from strain SK3981 and later pTrX BL21 (DE3) and has a SA of 40 units·mg^{-1} (*31*, *32*). *E. coli* thioredoxin reductase (TRR) was isolated from strain pMR14 K91 and has a SA of 1600 units·mg^{-1} (*33*). *E. coli* R1 was purified as previously described (*34*) and has a SA of 1200−3000 nmol·min^{-1}·mg^{-1} using a spectrophotometric assay as previously described (*35*). R1 concentration was determined using $\epsilon_{280\ nm}$ = 189 mM^{-1}·cm^{-1}. Pre-reduced R1 was generated by incubation of 10−60 μM R1 with 20 or 30 mM DTT for 20 min at 25 °C. At the end of incubation, hydroxyurea was added to final concentration of 20 mM, and the reaction mixture was incubated for another 5 min. This procedure is required to reduce the Y• in the trace amounts of R2 that always co-purifies with R1. R1 was then desalted on a Sephadex G-25 column. Preoxidized R1 was prepared as previously described (*34*). *E. coli* R2 was isolated as previously described and has a SA of 5000−8000 nmol·min^{-1}·mg^{-1} (*36*). R2 concentrations were determined using $\epsilon_{280\ nm}$ = 130.5 mM^{-1}·cm^{-1} and typically contained 0.9−1.3 equiv of Y• per dimer. All R1 and R2 concentrations are reported per dimer.

Preparation of [2-^{14}C]-CDP. [2-^{14}C]-CDP was synthesized enzymatically from [2-^{14}C]-cytidine using human deoxycytidine kinase (dCK) and myokinase. The expression vector for human dCK was a gift from Dr. Stefan Eriksson. Human dCK (SA = 150 nmol·min^{-1}·mg^{-1}) was isolated as previously described (*37*). [2-^{14}C]-Cytidine (250 μCi, 55 mCi/mmol, 4.5 μmol) was diluted with 23.5 μmol of cytidine to a SA of ∼20 000 cpm/nmol. The dCK reaction contained in a final volume of 28.0 mL: 1.0 mM [^{14}C]-cytidine (250 μCi, 28.0 μmol), 2.0 mM ATP, 0.50 mg/mL bovine serum albumin, 2.0 mM DTT, and 3.1 mg human dCK in 50 mM Tris-HCl, 100 mM KCl, 5 mM $MgCl_2$, pH 7.6. The reaction was incubated at 37 °C for 3 h. The mixture was then loaded onto a DEAE Sephadex A-25 column (2.5 × 10.3 cm) and eluted with a 425 × 425 mL linear gradient of 0.1−0.6 M triethylammonium bicarbonate, pH ∼7.2 (TEAB). Fractions containing [^{14}C]-CMP were pooled and evaporated to dryness to remove TEAB. Conversion of CMP to CDP was carried out in a final volume of 28.0 mL containing 1.0 mM [^{14}C]-CMP (SA 1.75 × 10^4 cpm/nmol), 24.5 mM dATP (pH readjusted to 7.5), and 4000 units of myokinase (2.3 mg) in 80 mM Tris-HCl, 40 mM KCl, 10 mM $MgCl_2$, pH 7.5. The reaction proceeded for 30 min at 37 °C and was then diluted with 1.0 M TEAB, pH 9.0, to ∼100 mL (∼0.7 M TEAB final), before loading onto a Boronate Affi-Gel 601 column (2.5 × 9.3 cm, binding capacity of ∼0.70 μmol/mL) preequilibrated with 1.0 M TEAB, pH 9.0. The column was washed with 4 column volumes of the same buffer and then eluted with CO_2-acidified H_2O. Fractions containing radioactivity were pooled and evaporated to dryness to remove TEAB. The residue was redissolved in 50 mM TEAB, loaded onto a DEAE Sephadex A-25 column (2.5 × 10.3 cm), and eluted with a 400 × 400 mL linear gradient of 0.1−0.6 M TEAB. [^{14}C]-CDP eluted at 0.35 M TEAB. The pooled fractions were evaporated to dryness, redissolved in 1:1 mixture of ethanol and H_2O, and re-evaporated ≥3 times to remove TEAB. [^{14}C]-CDP (λ_{max} = 269 nm, λ_{min} = 247 nm) was redissolved in 1.2 mL of 20 mM HEPES, 6 mM $MgSO_4$, 0.4 mM EDTA, pH 7.6, and loaded onto a Sephadex G-25 column (1.5 × 20 cm) equilibrated with the same buffer. Fractions containing [^{14}C]-CDP were pooled, evaporated, and redissolved in 1.5 mL of H_2O to give 18.1 μmol (65% yield, SA 1.80 × 10^4 cpm/nmol) in 360 mM HEPES, 108 mM $MgSO_4$, 7.2 mM EDTA, pH 7.6. Judging from a λ_{max} of 270 nm and a λ_{min} of 249 nm, little dADP, if any, was present in the final [^{14}C]-CDP. The product was analyzed by HPLC on a Partisil 10 SAX column (Whatman, 4.6 × 250 mm). [^{14}C]-CDP constituted 90.5% of total radioactivity. A late migrating peak accounted for another 8.2% of radioactivity. Before use, nonradioactive CDP was added to give a final SA of 4000−8000 cpm/nmol.

Y• of R2 Monitored by SF-UV/Vis Spectroscopy. Experiments were performed on an Applied Photophysics SX.18MV SF-UV/Vis instrument equipped with a Xenon arc lamp and a Lauda RM6 circulating water bath (Brinkmann). The Y• of R2 was monitored at 404, 410, and 414 nm at 25 °C using a $A_{410\ nm}$ dropline formula [$A_{410drop} = A_{410} \pm ((2 \times A_{404} + 3 \times A_{414})/5)$] as previously described (*38*). In a typical experiment, syringe A contained 30 μM R1, 3.2 mM ATP, 2.0 mM CDP, and was mixed with an equal volume of solution from syringe B that contained 30 μM R2 (1.1−1.3 Y•) in 50 mM HEPES (pH 7.6), 15 mM $MgSO_4$, 1.0 mM EDTA. The effect of reductant was measured in a second set of experiments. Syringe A contained 2.0 mM NADPH in addition to the contents listed above, while syringe B contained 250 μM TR and 5.0 μM TRR in addition. The effect of the allosteric effector was examined in a third set of experiments. Syringe A contained 6.0 μM R1, 33 μM R2 (1.2 Y•), and the contents were mixed with the solution from syringe B containing 2.2 mM CDP but no ATP in 50 mM HEPES (pH 7.6), 15 mM $MgSO_4$, 1.0 mM EDTA. Similar experiments were carried out at 2 °C and 12 °C and at pH 6.6. In addition, experiments were carried out with UDP (2.0 mM) and 0.09 mM TTP, with ADP (1.0 mM) and 0.1 mM dGTP, with [3′-^{2}H]-UDP, and in the presence of D_2O.

dCDP Formation Monitored by Rapid Chemical Quench. Rapid chemical quench experiments were performed at 25 °C on a KinTek RQF-3 instrument equipped with a Lauda RM6 circulating water bath. The mixing conditions are summarized in Table 1. Experiments were performed at final concentrations of 15 μM R1, 15−33 μM R2, 1.6 mM ATP (or 3 μM R1, 6 μM R2, 3 mM ATP), and 1.0 mM [^{14}C]-CDP in 50 mM HEPES, 15 mM $MgSO_4$, 1.0 mM EDTA, pH 7.6. Under multiple-turnover conditions, TR, TRR, and NADPH were included to give final concentrations of 40 μM, 0.8 μM, and 1.0 mM, respectively. In a separate experiment, the role of the allosteric effector was tested by omitting ATP. Typically 28 or 40 μL from each syringe were mixed and quenched with 197 μL of 2.0% $HClO_4$. The reaction time varied from 5.0 ms to 5 min. The zero time point was generated by placing buffer in syringe B. Triplicate runs were performed for each time point. Immediately after quenching, 0.4 M KOH (185 μL) was added to neutralize each solution. Samples were maintained on ice until the completion of the entire time course. At this time, calf

Table 1: Mixing Conditions and Results of Rapid Chemical Quench Experiments

exp.	syringe A	syringe B	dCDP/R1, before exp	dCDP/R1, after exp	k_{obs}	burst phase amplitude
1	6 μM R1, 6.0 mM ATP, 2.0 mM [^{14}C]-CDP	12.0 μM R2 (1.2 Y$^{\bullet}$)	3.1,[a] 2.8[b]	ND	10.3 s^{-1}	2.16 equiv
2	30 μM R1, 3.2 mM ATP, 2.0 mM [^{14}C]-CDP	30 μM R2 (0.9 Y$^{\bullet}$)	3.1,[a] 3.3[b]	3.2[b]	6.5 s^{-1}	ND
3	30 μM R1, 3.2 mM ATP, 2.0 mM [^{14}C]-CDP	65 μM R2 (0.9 Y$^{\bullet}$)	3.0, 2.9[b]	2.8[b]	8.0 s^{-1}	1.55 equiv
4	30 μM R1, 3.2 mM ATP, 2.0 mM [^{14}C]-CDP	60 μM R2 (1.0 Y$^{\bullet}$)	3.4,[a] 3.0[b]	3.0[a]	16.5 s^{-1}	1.88 equiv
5	30 μM R1, 30 μM R2 (0.9 Y$^{\bullet}$), 40 μM TR, 1.6 μM TRR, 2.0 mM NADPH	3.2 mM ATP, 2.0 mM [^{14}C]-CDP, 40 μM TR	ND	ND	5.2 s^{-1}	ND
6	30 μM R1, 3.2 mM ATP, 2.0 mM [^{14}C]-CDP, 2.0 mM NADPH	65 μM R2 (0.9 Y$^{\bullet}$), 80 μM TR, 1.6 μM TRR	ND	ND	6.1 s^{-1}	1.34 equiv
7	30 μM R1, 30 μM R2 (1.0 Y$^{\bullet}$)	3.2 mM ATP, 2.0 mM [^{14}C]-CDP	3.6,[a] 3.2[b]	2.9[a]	4.4 s^{-1}	ND
8	30 μM R1, 3.2 mM ATP	30 μM R2 (0.9 Y$^{\bullet}$), 2.0 mM [^{14}C]-CDP	3.4[b]	2.8[b]	6.4 s^{-1}	ND
9	30 μM R1, 30 μM R2 (0.9 Y$^{\bullet}$), 200 μM TTP	2.0 mM [^{14}C]-CDP	3.0, 3.1[b]	2.9[b]	4.2 s^{-1}	ND
10	30 μM R1, 2.0 mM [^{14}C]-CDP	65 μM R2 (0.9 Y$^{\bullet}$)	2.5[c]	ND	2.2 s^{-1}	1.35 equiv
11	30 μM R1 C754S/C759S, 3.2 mM ATP, 2.0 mM [^{14}C]-CDP	60 μM R2 (1.2 Y$^{\bullet}$)	1.7[a]	ND	20.9 s^{-1}	1.90 equiv
12			1.7[a]	1.9[b]	20.0 s^{-1}	1.48 equiv
13	30 μM R1 C754S/C759S, 3.2 mM ATP, 2.0 mM [^{14}C]-CDP	30 μM R2 (1.2 Y$^{\bullet}$)	2.1, 2.0,[b] 1.4[a] 2.0, 1.8[b]	1.8, 1.6[b]	12.5 s^{-1}	1.37 equiv

[a] Hand quench. [b] Equal volumes of samples from each syringe were mixed and quenched on rapid chemical quench apparatus. [c] Sample quenched on rapid chemical quench apparatus after 10 min. ND, not determined.

intestine alkaline phosphatase (20 U) and 400 nmol of carrier deoxycytidine (dC) in 1.0 M Tris-HCl, 10 mM EDTA, pH 8.5, were added to each sample to give a solution of 100 mM Tris-HCl, pH ~ 8. The mixtures were incubated at 37 °C for 2 h. dC and cytidine were separated on Dowex-1 borate columns by the procedures of Steeper and Steuart (*39*). One mL of the 12 mL eluent was mixed with 9 mL of Emulsifier-Safe scintillation fluid (Packard) and analyzed for radioactivity on a Beckman LS 6500 Scintillation Counter.

Preparation and Characterization of C754S/C759S−R1. C754S/C759S−R1 was purified as previously described from BL21(DE3) containing pMJ1 C754S/C759S (*18*). A typical assay contained in a volume of 0.46 mL: 1.0 μM R1 C754S/C759S, 5.0 μM R2, 1.6 mM ATP, 1.0 mM [^{14}C]-CDP, and 20 mM DTT in 50 mM HEPES (pH 7.6), 15 mM $MgSO_4$, 1.0 mM EDTA. Aliquots (100 μL) were taken from 0 to 15 min and quenched by immersion in a boiling water bath. The C754S/C759S−R1 mutant exhibited a SA of 46−59 nmol·min^{-1}·mg^{-1}. Wt R1 under the same conditions exhibited a SA of 83−95 nmol·min^{-1}·mg^{-1}. In the absence of any external reductant, pre-reduced C754S/C759S−R1 produced 1.4−1.7 equiv of dCDP after 5 min incubation with equimolar R2, 1.6 mM ATP, and 1.0 mM [^{14}C]-CDP under conditions identical to those used in the assay.

dCDP Formation with C754S/C759S−R1 Monitored by Rapid Chemical Quench. Rapid chemical quench experiments were carried out with C754S/C759S−R1, ATP, and [^{14}C]-CDP in syringe A and R2 in syringe B. The final concentrations were 15 μM C754S/C759S−R1, 15 μM R2 (1.1 Y$^{\bullet}$), 1.6 mM ATP, and 1.0 mM [^{14}C]-CDP in 50 mM HEPES buffer (pH 7.6), 15 mM $MgSO_4$, 1.0 mM EDTA. Samples were quenched and analyzed as described above.

dCDP Formation with Preoxidized R1 Monitored by Rapid Chemical Quench. Syringe A contained 30 μM preoxidized R1, 65 μM R2, and 5.0 μM TRR, and syringe B contained 3.2 mM ATP, 2.0 mM [^{14}C]-CDP, 250 μM TR, and 2.0 mM NADPH. The concentrations of TR and TRR were chosen such that the rate of NADPH consumption using the spectrophotometric assay under identical conditions was saturated with regard to TR and TRR. Equal volumes of solution from each syringe were rapidly mixed, and samples were quenched and analyzed as described above.

Data Analysis. Curve fitting was performed using the program KaleidaGraph. For data points between 0 and 400 ms, product formation in the absence of external reductant (single turnover conditions) was fit with a single-exponential function $y = A \times [1 - \exp(-k_{obs}t)]$, where A represents the amplitude and k_{obs} is the observed rate constant. For data points collected over a 0−5 min time course, data were fit with a double exponential function $y = A_1 \times [1 - \exp(-k_1t)] + A_2 \times [1 - \exp(-k_2t)] + c$, where A_1 and A_2 represent amplitudes, k_1 and k_2 are the rate constants for each kinetic phase, and c is a constant. Under multiple turnover conditions, product formation was fit with the equation $y = A \times [1 - \exp(-k_{obs}t)] + k_{linear}\cdot t + c$, where k_{linear} is k_{cat} for the steady-state turnover and c is a constant. Rates of product formation with preoxidized R1 were fit using the program Dynafit (*40*) and the kinetic mechanism in Figure 1. The best fit to the lag phase required a minimum of two slow steps for the re-reduction of the active site disulfide.

Activity of R1 and R2: Evidence for Y$^{\bullet}$ Reduction and Reoxidation on Each Turnover. The turnover numbers of R1 and R2 were determined independently using the coupled assay with *E. coli* TR and TRR monitoring NADPH consumption at 340 nm at 25 °C. R1 (0.01−3.0 μM) was assayed with a 5-fold molar excess of R2. Conversely, R2 (0.01−2.0 μM) was assayed with a 5-fold excess of R1. All assay mixtures contained in a volume of 0.35 mL: 1.6 mM ATP, 1.0 mM CDP, TR, TRR, and 1.0 mM NADPH in 50 mM HEPES (pH 7.6), 15 mM $MgSO_4$, 1.0 mM EDTA. TR and TRR were 40 and 1.6 μM, respectively, when the concentrations of R1 and R2 were in the range of 0.01 to

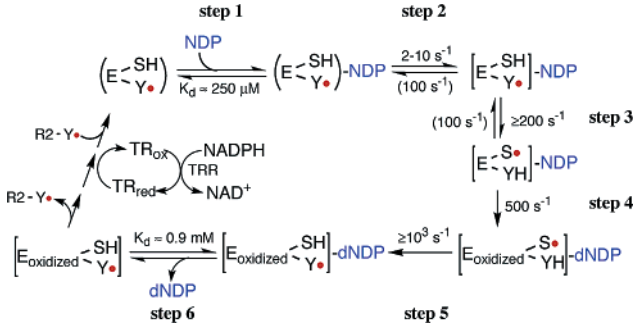

FIGURE 1: Proposed kinetic mechanism of the *E. coli* class I RNR. (E) and [E] represent two different enzyme conformations of RNR, the latter being the "active" conformation. SH represents C439 on R1, Y• represents Y122 on R2. Step 1, K_d from the work of von Dobeln and Reichard (*53*). Step 2, this work. Steps 3 and 4, modeled rate constants are required to account for our inability to detect any changes in the Y• signal (<5%), the lack of a V_{max} isotope effect on nucleotide reduction, and V/K isotope effects observed with [3′-^{2}H]-NDP as substrate (*41*). Step 5, the irreversibility of this step is based on studies from Stubbe et al. (*41*). Step 6, the K_d from the work of Allard et al. (*49*). The rate constants given in parentheses are representative values that are able to account for the experimental data using kinetic simulations (*65*).

0.2 μM. At higher RNR concentrations, TR and TRR concentrations were scaled proportionally. At 3.0 μM R1, 15 μM R2, TR and TRR concentrations were 600 and 24 μM, respectively. When the reaction was too fast to be monitored by hand mixing, NADPH consumption was measured by SF-UV/vis spectroscopy at 25 °C.

RESULTS

Pre-Steady-State Experiments Monitoring Changes in the Y•. Our efforts to understand radical initiation in the class I RNRs, that is, PCET, requires an understanding of which step (or steps) are rate-limiting in this system. Our favored mechanistic hypothesis for the class I RNR is developed from the structural and functional congruence of the class I and II RNRs and their similar turnover numbers (2−10 s^{-1}). The *Lactobacillus leichmannii* RNR is monomeric and uses NTPs as substrates. Mechanistic studies using site-directed mutants, mechanism-based inhibitors, and the normal substrate with the wt enzyme have established striking similarities between this class II RNR and the *E. coli* class I RNR. In the *L. leichmannii* RNR, the rate-limiting step has been established as the re-reduction of the active site or peripheral disulfides or a conformational change associated with these steps (*7*). Furthermore, in this class II RNR, the homolysis of the carbon−cobalt bond of AdoCbl (the radical initiator) and its re-formation was readily observed ($k_{apparent}$ of 250 s^{-1} and 30 s^{-1}, respectively) (*7*−*12*). Thus, if the class I RNR behaves in a similar fashion, one might expect to observe the disappearance and re-appearance of the Y• on R2 (Scheme 1). This radical is detectable by electron paramagnetic resonance (EPR) spectroscopy and by visible spectroscopy, as it has a sharp absorption feature at 410 nm. Both spectroscopic methods are amenable to monitor changes in its redox state. We chose to use SF-vis methods to monitor changes in the Y• in the pre-steady state under a wide range of conditions. No changes in the Y• were observed between 2 ms and minutes regardless of the substrate (UDP, CDP, ADP) used, or whether the appropriate allosteric effector (ATP, TTP, dGTP) was present (data not shown). In addition, no changes were observed under multiple turnover conditions using TR/TRR/NADPH or DTT as reductant. In an effort to slow the chemistry, [3′-^{2}H]-UDP was used as a substrate, experiments were carried out in D_2O, and the pH of the reaction mixture was lowered to 6.6 (at this pH, the rate of RNR is 30% of that at pH 7.6). The reaction temperature was also varied from 2 to 25 °C (*41*, *42*). No changes in the Y• were detected under any of these conditions. The simplest model that accommodates inability to detect changes in the Y• concentration is that a physical step prior to radical initiation is rate-limiting and that Y• reduction, the nucleotide reduction chemistry, and Y reoxidation are all rapid (Figure 1). Thus, even though the Y• is reduced and reoxidized, this change is kinetically invisible. This model further predicts that the rate constant of disulfide formation and dNDP formation in the pre-steady state should be identical to each other [limited by the conformational change(s)] and to the rate constant for deoxynucleotide formation in the steady state (k_{cat}).

Quality Control of the Reduction State of R1 during Pre-Steady-State Rapid Chemical Quench Experiments. Before embarking on measurement of deoxynucleotide formation in the pre-steady state, the sensitivity of the active site (C225, C462) and peripheral cysteines (C754, C759) in R1 to spontaneous oxidation was determined. An experiment in which R1 had been pre-reduced and no external reductant was added (single turnover conditions) could yield up to 4 dCDPs when incubated in the presence of R2 and CDP. Experimentally, we found that only 3.0−3.5 dCDPs are generated, possibly due to our inability to completely reduce R1, folding problems with recombinant R1, or the sensitivity of the catalytic cysteines in R1 to oxidation (*18*). A set of control experiments to monitor oxidation therefore accompanied each pre-steady-state experiment described in the following sections. Formation of dCDP was monitored in the beginning and upon completion of each set of experiments. A typical set of rapid chemical quench experiments can take up to 1 h. The results of many experiments are summarized in Table 1. They demonstrate that, at the start of an experiment, usually as soon as R1 is pre-reduced, 2.8−3.5 equiv of dCDP is observed, and at the end of a set of experiment, 2.8−3.0 equiv of dCDP is observed. Thus R1, as we have observed, is never in the completely reduced state, and 10−20% oxidation can occur over the course of a chemical quench experiment. Similar experiments were carried out with C754S/C759S−R1 (Scheme 2) in which a theoretical maximum of 2 dCDPs could be generated. The results showed 1.4−2.0 equiv of product formation before an experiment and 1.6−1.9 equiv at the end of an experiment (Table 1). Thus the peripheral cysteines (which are mutated in C754S/C759S−R1) appear to be more sensitive to oxidation relative to the active site cysteines. Finally, the number of dCDPs generated by R1 in these control experiments (that is, over extended incubation times) should not be confused with our kinetic model in which dCDPs are monitored on millisecond to second time scale.

An additional quality control issue should be noted. Despite the fact that R2 is a homodimer, the recombinant protein isolated in many different labs contains 0.9 to 1.3 Y•s. The number of radicals per dimer *in vivo* is unknown. This stoichiometry has implications, as noted above, in any model for an R1−R2 complex and its ability to produce dNDPs in a single turnover (no external reductant).

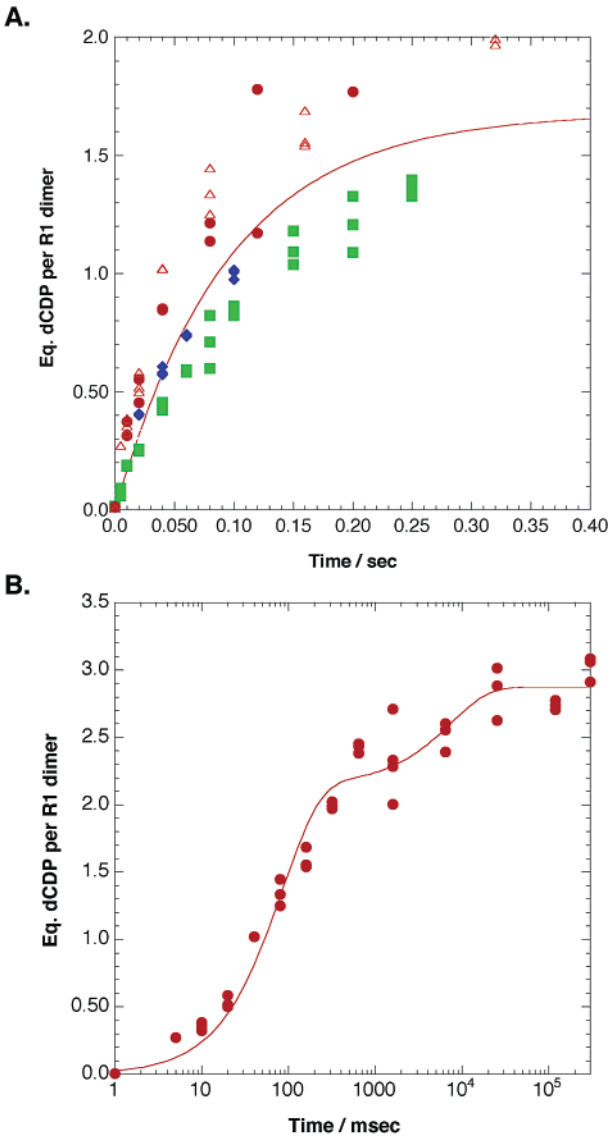

FIGURE 2: Rapid chemical quench experiments monitoring dCDP formation using wt RNR. (A) dCDP formation in the pre-steady state under conditions described in Table 1: exp 1, orange triangles; exp 2, blue diamonds; exp 3, green squares; and exp 4, red circles. (B) Reaction carried out for a longer time period (note the logarithmic time scale). dCDP formation in the pre-steady state under conditions in Table 1, exp 4.

dCDP Formation under Pre-Steady-State Conditions. Having established the maximum number of dCDPs that can be generated by RNR, experiments to monitor dCDP formation on millisecond to second time scale have been carried out. If the rate-limiting step precedes deoxynucleotide formation, then the rate of product formation should be governed by this step and be the same as the steady-state k_{cat}. If, instead, the rate determining step occurs after the nucleotide reduction chemistry, then the pre-steady-state rate of dCDP formation should be faster than the rate measured in the steady state. Rapid mixing of R1, ATP, and [^{14}C]-CDP with an equal volume of solution containing R2 (0.9−1.3 equiv of Y$^{\bullet}$) gave results shown in Figure 2A. Analysis of multiple data sets using many different preparations of enzymes gave a rapid phase of dCDP formation with k_{obs} of 9 ± 4 s^{-1} and an amplitude of 1.7 ± 0.4 equiv of dCDP per R1 dimer (Table 1, average of exp 1−6). The presence or absence of the reducing system (TR/TRR/NADPH) did not significantly affect the rate constant of this phase (Table 1, compare exp 2−4 and 5, 6). Furthermore, similar rate constants were measured at 3 μM (10 s^{-1}, Table 1, exp 1) and 15 μM enzyme concentrations (9 ± 5 s^{-1}, Table 1, exp 2−6) within the range of error. Additional experiments carried out in the absence of effector ATP gave k_{obs} of 2 s^{-1} (Table 1, exp 10 and Figure 3). The rate constants for dCDP formation in these experiments are very similar to the turnover number of RNR in the presence of effector (k_{cat} of 10 s^{-1} and 14 s^{-1}, Figure 6) and in the absence of effector (k_{cat} of 2 s^{-1}) obtained from steady-state experiments under standard assay conditions (0.05−0.4 μM). The similarities in the rate constants for dCDP formation between the pre-steady-state and steady-state experiments, as well as our inability to detect changes in the Y$^{\bullet}$ under similar conditions, support the model that a conformational step prior to radical initiation and the chemistry is rate-limiting.

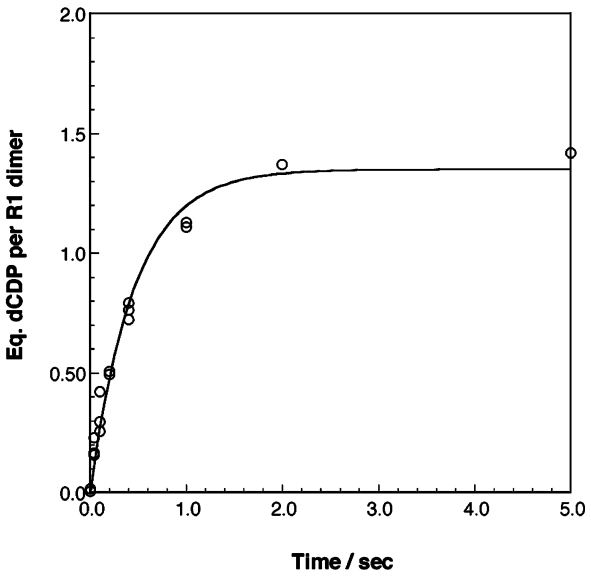

FIGURE 3: Rapid chemical quench experiments monitoring dCDP formation in the absence of effector ATP using wt RNR. Final concentrations were 15 μM R1, 33 μM R2, and 1.0 mM CDP. The data were fit to a single-exponential function (solid line), giving a k_{obs} of 2.2 s^{-1} and an amplitude of 1.35 equiv

Can Effectors or Substrate Gate the Conformational Changes that Limit dNDP Formation? If binding of substrate or an allosteric effector (ATP or TTP) to the R1R2 complex, or R2 binding to R1 is slow, then different kinetics of dCDP formation could be observed in the pre-steady state under different mixing conditions. The results of several experiments to test this hypothesis are presented in Table 1 (exp 1−9). Similar rate constants were observed under all mixing conditions, given the error in the data. The similarities in the k_{obs} provide the first indication that the rate-limiting step occurs after the assembly of the R1−R2−substrate ternary complex, or the quaternary complex of R1−R2−effector−substrate. These results further support a rate-limiting conformational change required to trigger PCET. Unfortunately, steady state kinetic experiments using a coupled spectrophotometric assay with TR, TRR, and monitoring NADPH consumption, are sufficiently complex that the order of addition and dissociation of all the components cannot be determined [Chalfoun and Stubbe, unpublished results, and Thelander (*43*)].

Multiphasic Kinetics of dCDP Formation under Single Turnover Conditions. As noted above, pre-reduced R1 in the absence of external reductant, when incubated with R2 and CDP for 5 min gave rise to 2.8−3.5 equiv of dCDP. In the rapid phase (200 ms, Figure 2A) of the pre-steady-state experiments, however, only 1.7 ± 0.4 equiv of dCDP (Table 1, Scheme 2B) was formed. Thus experiments were carried out for a longer time period to look for the missing dCDPs. In the absence of any external reductants, a second kinetic phase, or phases, with an amplitude of 0.8 equiv of dCDP was observed, giving a total of 3.0 ± 0.2 equiv (Figure 2B). The number of 3 dCDPs agrees with our control experiments (Table 1) and earlier studies by Thelander (*43*). As noted above, oxidation of R1, or inability to completely reduce R1, is likely responsible for the observed stoichiometry. The scatter in the data makes it impossible to obtain a good rate constant for the slow phase; however, the rate constant (on the order of 0.1 s^{-1}) is clearly much slower than the steady-state k_{cat} of 1.0 s^{-1} observed at the same enzyme concentration (15 μM) [note, as discussed subsequently, that the turnover numbers for dCDP formation vary with the concentration of R1 and R2 in an unusual fashion]. Thus nucleotide reduction in this phase(s) is not kinetically competent for normal catalysis. The observation of a rapid phase of deoxynucleotide formation followed by a second slow kinetic phase is very similar to the results of analogous experiments carried out with the monomeric *L. leichmannii* RNR. This enzyme (structurally homologous to the class I RNR) (*44*) also possesses two pairs of redox cysteines per polypeptide chain. In the absence of any reducing system, the enzyme rapidly produces 0.7−0.8 equiv of deoxynucleotide product and, at longer incubation time, gives a total of 1.6 equiv of product (*45*). The amount of dCDP produced by the *E. coli* class I RNR in each kinetic phase supports the model in Scheme 2B, in which both monomers of R1 are active.

dCDP Formation with C754S/C759S−R1 Mutant. The complexity of dCDP stoichiometry and the observation of two kinetically distinct phases of product formation (Figure 2B) raised the question of which pairs of cysteines are oxidized in each kinetic phase. Our model (Scheme 2B) requires that each pair of active site cysteines (C225, C462) of R1 is oxidized to generate 2 dCDPs in the rapid kinetic phase. The model (Scheme 2A) requires that only one active site in the R1 dimer is active, but that 3 dCDPs can be produced in a single kinetic phase due to rapid disulfide interchange with the peripheral cysteines in each monomer (Scheme 2A) (*29*).

As a direct test of the model in Scheme 2A, a pre-steady-state experiment with C754S/C759S−R1 has been carried out. This model requires that this mutant should generate only 1 equiv of dCDP in the rapid kinetic phase under pre-steady state conditions, given that only one active site participates in catalysis. The results of three experiments are shown in Figure 4. The observation of 1.6 ± 0.3 equiv of dCDP formed with a rate constant of 18 ± 4 s^{-1} (Table 1, average of exp 11−13) indicate the model in Scheme 2A cannot be correct.

Rapid Chemical Quench under Multiple Turnover Conditions: A Second Rate Determining Step. In contrast to the time course of dCDP formation observed with pre-reduced R1 in the absence of reductant (Figure 2B), in the presence

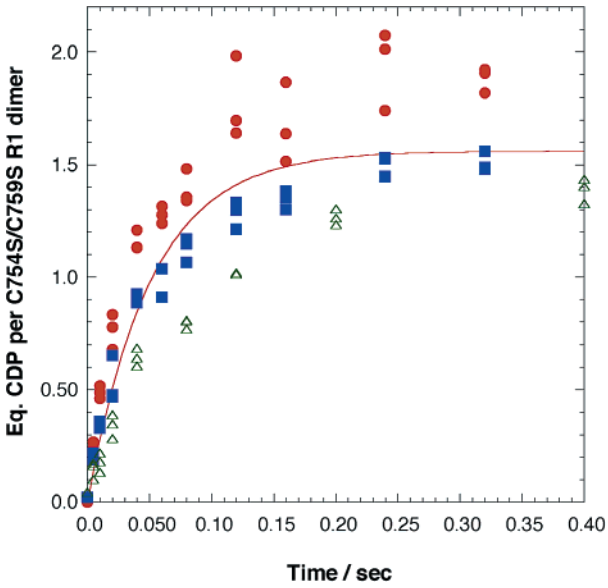

FIGURE 4: dCDP formation in the pre-steady state using C754S/C759S−R1. In the rapid chemical quench experiments, C754S/C759S−R1, ATP, and CDP were mixed with an equal volume of R2 to give final concentrations of 15 μM C754S/C759S−R1, 30 μM R2 (Table 1, exp 11, red circles), or 15 μM R2 (exp 12, blue squares; exp 13, green triangles), 1.6 mM ATP, and 1.0 mM CDP.

of the reducing system TR/TRR/NADPH, a linear phase with a rate constant of 0.9 s^{-1} follows the rapid phase (Figure 5A). The rate constants for the rapid phase in both experiments are identical within experimental errors (Table 1). The rate constant for the slow phase, 1 s^{-1}, however, is much slower than the steady-state turnover of 10−14 s^{-1} measured under typical assay conditions of 0.05−0.4 μM enzyme. Thus a coupled spectrophotometric assay using TR/TRR/NADPH was carried out under conditions identical to the rapid chemical quench experiments (15 μM RNR). The turnover number under these conditions is 1.0 s^{-1}, in agreement with the rapid chemical quench experiments. The observed dependence of turnover number on the concentrations of R1 and R2 is addressed subsequently. These results suggest that, under nonphysiological concentrations, the rate-determining step has changed and is now associated with re-reduction of the disulfide generated during nucleotide reduction. This process may well be effected by the protein concentration, as R2 may be required to dissociate from R1 in order to allow the access of the reductant TR to the peripheral disulfide (C754−C759). This model is appealing in that the structurally homologous class II monomeric RNR, as noted above, has a turnover number of 2 s^{-1} that is also limited by disulfide re-reduction (*1*).

Rapid Chemical Quench Experiments with Fully Oxidized R1. To obtain support for the hypothesis that re-reduction of R1 can be rate-limiting under conditions in which R1 and R2 are present at high concentrations, preliminary studies to monitor the reduction of oxidized R1 by the TR/TRR/NADPH system were undertaken. Starting from fully oxidized R1, several steps, including the reduction of peripheral disulfide by TR, disulfide interchange (resulting in the reduction of active site disulfide, C225−C462, and reoxidation of C754/C759 dithiol), and possibly re-reduction of the peripheral disulfide, are minimally required before CDP reduction can take place (*18*). dCDP formation was thus monitored by rapid chemical quench experiments in which

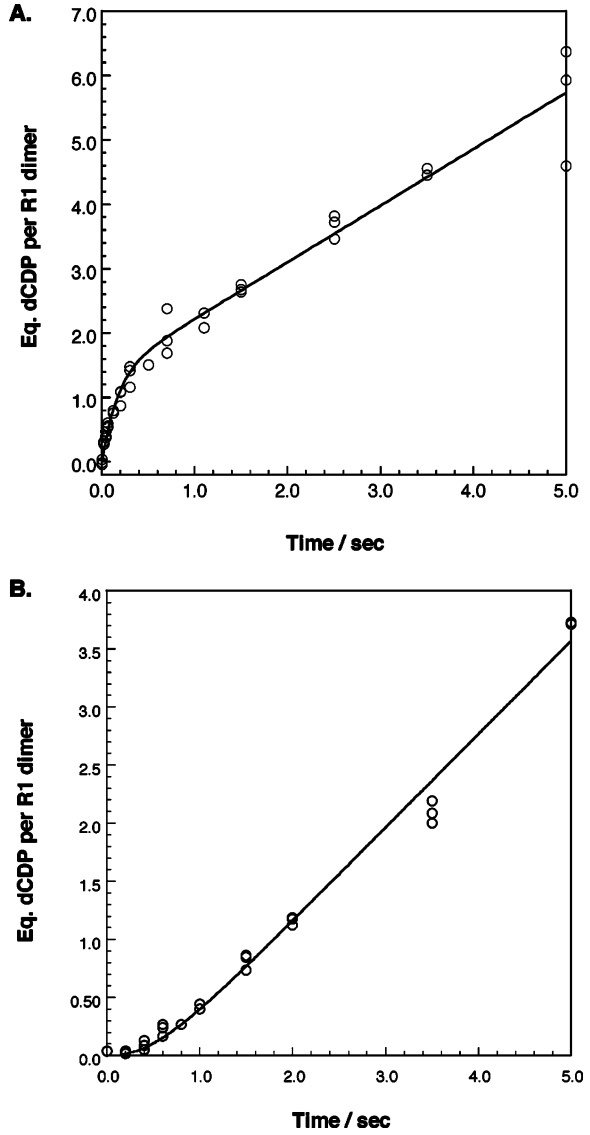

FIGURE 5: (A) dCDP formation measured under multiple turnover conditions. Final concentrations were 15 μM R1, 33 μM R2, 1.6 mM ATP, 1.0 mM CDP, 40 μM TR, 0.8 μM TRR, and 1.0 mM NADPH (Table 1, exp 6). (B) dCDP formation with preoxidized R1 under multiple-turnover conditions. In this experiment, oxidized R1, R2, and TRR were mixed against ATP, CDP, TR, and NADPH to give final concentrations of 15 μM R1, 33 μM R2, 1.6 mM ATP, 1.0 mM CDP, 125 μM TR, 2.5 μM TRR, and 1.0 mM NADPH.

preoxidized R1, R2, and TRR were mixed with ATP, CDP, TR, and NADPH. The results, shown in Figure 5B, display a lag phase in dCDP formation, followed by a linear steady state with a rate constant of 0.9 s^{-1}. Kinetic modeling (Figure 1) using Dynafit (*40*), in which the lag phase involves two slow steps with rate constants of 1.7 s^{-1}, followed by a physical step of $\sim$10 s^{-1}, can account for the observed kinetics and the steady-state turnover of 0.9 s^{-1}. Therefore, fully oxidized R1 can be a kinetically viable intermediate in the reaction cycle of RNR. The observation of a lag phase further corroborates the presence of slow step(s) in the re-reduction of R1 at high enzyme concentrations employed in these chemical quench experiments. These results, i.e., detection of a lag phase followed by a linear rate approaching that observed in the steady state, are also very similar to those observed with oxidized *L. leichmannii* RNR.

Steady-State Kinetics in Conjunction with Pre-Steady-State Experiments Support a Model in which Y• in R2 is Oxidized and Reduced during Each Turnover. Our steady-state kinetic studies on the class II RNR, which utilizes AdoCbl as radical initiator, have revealed that the carbon−cobalt bond of AdoCbl is cleaved and re-formed on every turnover (*7*). The weak binding of AdoCbl to RTPR (K_d > 100 μM) is unusual for such a large molecule and is consistent with AdoCbl being able to service more than one RTPR before the peripheral disulfide is converted to a form capable of further deoxynucleotide formation. Steady-state experiments modeled after those carried out with the class II enzyme have been performed in an effort to understand if reduction and reoxidation of the Y• on R2 occurs during each turnover.

As with AdoCbl for RTPR, R2 has a weak affinity for R1 (K_d of 0.2 μM).(*46, 47*) This weak affinity is the basis for the unusual conditions used to measure turnovers in the steady state. In a typical assay, the concentrations of R1 and R2 are in the range of 0.05−0.4 μM. To ensure that R1 and R2 form the "active" 1:1 complex, one subunit is always assayed in the presence of an excess of the other subunit with the excess used being based on the measured K_d for subunit interactions. The results of the experiments in which R1 is assayed in the presence of 5-fold excess of R2 and vice versa, however, do not give rise to the same turnover numbers (Figure 6A,B). A k_{cat} of 10 s^{-1} was obtained when R1 was the limiting reagent, compared to 14 s^{-1} for R2 (Figure 6A, B, inset) in the concentration range of 0.05−0.4 μM. In our lab over many years, different preparations of R1 and R2 have given variable k_{cat} values: 3−10 s^{-1} for R1 and 7−14 s^{-1} for R2. The turnover number of R2 is consistently higher than the turnover number of R1 at all protein concentrations. Similar observations have been reported by other laboratories.

The data in Figure 6 also reveal an unusual effect of enzyme concentration on k_{cat}. As first documented by Erickson (*30*), with increasing concentrations of R1 and R2, the k_{cat} values for both R1 and R2 increase, plateau and then decrease (Figure 6A,B). The initial increase in turnover numbers with increasing R1 or R2 concentrations (in the range of 0.01−0.4 μM) is presumably associated with complex formation between R1 and R2. At concentrations of R1 and R2 higher than 0.4 μM, the turnover numbers decrease. At 3 μM R1 and 15 μM R2, for example, the k_{cat} for R1 is 2.8 s^{-1}, reduced from the value of 10 s^{-1} observed in the range of 0.05−0.4 μM R1. At 15 μM R1 and 33 μM R2 (conditions used for some of the pre-steady-state experiments described above), k_{cat} further declines to 1.0 s^{-1}. This decline in turnover numbers may be associated in part with a change in the rate-limiting step at high protein concentrations and/or altered aggregation states of R1 (*22, 48*).

DISCUSSION

A Model to Accommodate the Kinetic Results. The radical initiation process in the class I RNRs remains a major unsolved mechanistic problem. Specifically, how the Y• on R2 is involved in generation of a transient S• on R1, and whether this process involves reversible long range PCET, is presently the focus of a number of laboratories. To design experiments to examine PCET requires an understanding of which steps are rate-limiting in the RNR catalyzed reaction

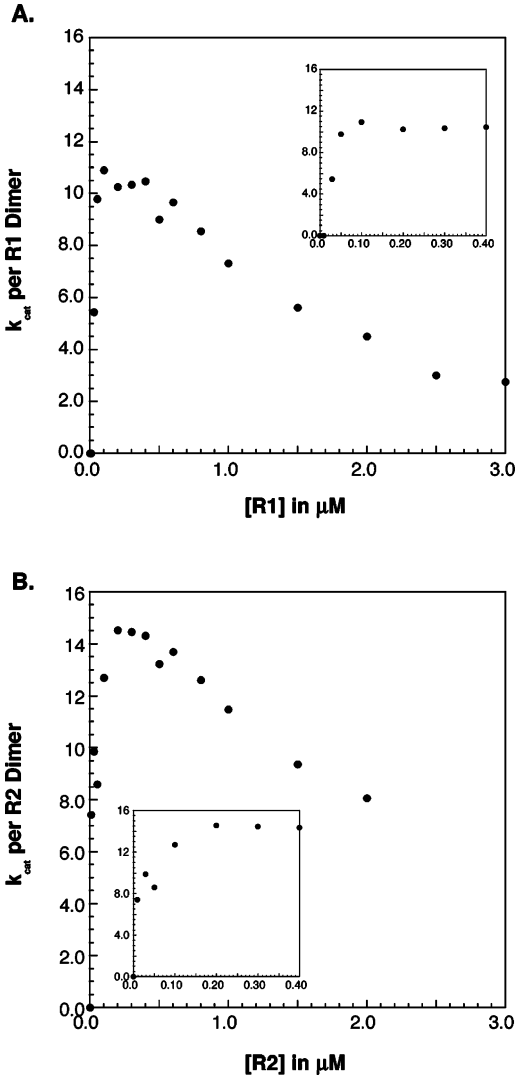

FIGURE 6: Steady-state kinetics of *E. coli* RNR using TR/TRR/NADPH as reducing system, measured by the spectrophotometric assay monitoring NADPH consumption at 340 nm. (A) R1 is assayed in the presence of 5-fold excess R2 at all concentrations indicated. The turnover number is calculated per R1 dimer (2 active sites). Inset: under dilute concentrations, k_{cat} per R1 = 10 s^{-1}. (B) R2 is assayed in the presence of 5-fold excess R1 at all concentrations indicated. Turnover number is calculated per R2 dimer (1.0 Y•). Inset: under dilute conditions, k_{cat} per R2 = 14 s^{-1}.

and, furthermore, requires an understanding of the interactions between the two subunits, and how they change in the presence of nucleotide substrate and effectors and as a function of the concentration of the proteins. Thus, this is a very complex system, and the pre-steady state and steady-state experiments presented here have provided a starting point for the formulation of our minimal mechanistic model (Figure 1).

Our pre-steady-state experiments, monitoring product (dCDP) formation and changes in Y• concentration, complement the pre-steady-state experiments of Erickson monitoring disulfide formation at the active site that accompanies dCDP formation (Scheme 2). The observation that no changes in the Y• concentration can be observed under a variety of conditions clearly limits our mechanistic options. In addition, the chemical mechanism for dCDP reduction requires that the rate of disulfide formation between C225 and C462 (Scheme 1) must be greater than or equal to the rate of dCDP formation. The values of 8 ± 3 s^{-1} and of 1.5 ± 0.2 s^{-1} for disulfide formation, measured in the presence and absence of effector ATP (*30*), respectively, agree with our findings of 9 ± 4 s^{-1} in the presence of ATP and 2.2 s^{-1} in the absence of the effector, determined at 3 and 15 μM R1 concentrations. The additional agreement between these k_{obs} values and the turnover numbers of R1 and R2 in the steady state under typical assay conditions (0.05−0.4 μM) suggests that a physical step prior to radical initiation and chemistry is rate-limiting under dilute enzyme conditions.

More recent pre-steady-state experiments by Erickson, in which disulfide formation between both C225−C462 and C754−C759 were measured (15 μM R1, 30 μM R2 and ATP), reported a rate constant of 2 s^{-1} for a single kinetic phase (*29*). This number is not kinetically competent, that is, it is too slow to be reconciled with our observed value of 9 ± 4 s^{-1} for dCDP formation under nearly identical conditions. In this second paper, Erickson reported problems with nonenzymatic oxidation of R1, consequently R1 was placed in a buffer at pH 6.5 in all of the experiments. This contrasts with the buffer conditions used in his first paper (pH 7.6) and in all of our experiments (*30*). As noted in Table 1, our control experiments revealed minimal oxidation of R1 during the period of the pre-steady-state experiments.

Erickson's studies with the antibodies to the peripheral cysteines led to his model in Scheme 2A, in which only one active site of the dimeric R1 was able to generate dCDP, and the peripheral cysteines from either monomer could rapidly re-reduce the active site disulfide in this one monomer, leading to the prediction that 3 dCDPs should be generated in a single kinetic phase. Our studies using the C754/C759S double mutant of R1, in which 2 dCDPs (Table 1, Figure 4) were generated, suggest that this model is not valid. At present, we do not understand the basis for the experimental observations in the second paper and the discrepancy between those and our results.

Nonetheless, our studies are consistent with the results of the first set of experiments reported by Erickson and together have led to an alternative model shown in Scheme 2B (*30*). This model requires that two dCDPs are formed rapidly in a single fast kinetic phase and that while re-reduction of the active site disulfides formed may well be rapid, in the absence of external reductant, the second set of dCDPs is generated at a rate that is not kinetically competent.

The pre-steady-state and steady-state experiments reported in this paper and our previous studies on the class I and II RNRs have resulted in our working kinetic model for subunit interactions, radical initiation, and nucleotide reduction shown in Figure 1 (*1*, *26*). The model has several steps and associated rate constants that are experimentally underdetermined, but is serving as a guide for future experiments and accommodates all known experimental facts about the system to date. First, rapid reversible binding of substrate, effectors, and products to R1 of RNR have previously been determined (steps 1 and 6) and are assumed to be the same in the presence of R2 in our kinetic model (*23*, *49*−*53*). Second, the rate-determining step from the present steady-state and pre-steady-state experiments is proposed to be a conformational change (step 2) triggered by ternary or quaternary complex formation (R1−R2−NDP or R1−R2−NDP−dNTP). Apparent rate constants of 2−10 s^{-1} have been measured in the absence and presence of allosteric

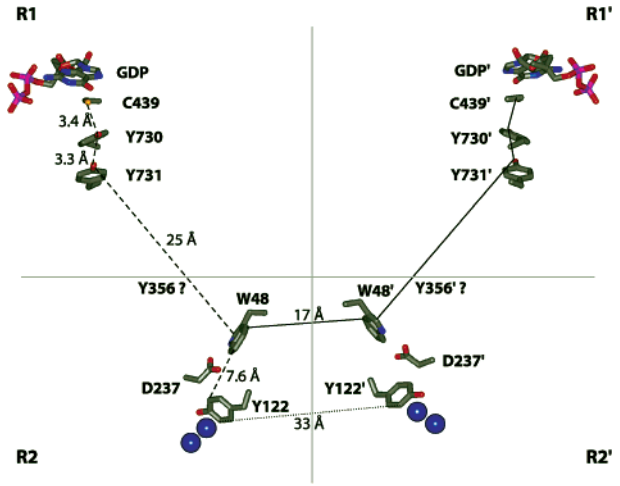

FIGURE 7: The proposed PCET pathway for the communication between each monomer of R1and R2 (*25*). As indicated by the solid line, an alternative ET pathway is proposed to account for the amplitude of the single-exponential phase of dCDP formation in the pre-steady state relative to the amount of Y•. In this case, ET may proceed from Y122 to W48 (monomer R2) to W48′ to Y356′ (monomer R2′) to Y731′, Y730′ to C439′ (monomer R1′).

effectors, respectively. The appropriate conformational change is proposed to trigger long-range PCET from the Y• on R2 to generate the transient S• on R1 (step 3). If this radical initiation process is in fact long range, then it must involve amino acid radical intermediates (*26*). The current models for PCET suggest that the distances between the intermediates are short, thus the PCET process would be rapid (>200 s^{-1}) and possibly limited by the conformational changes associated with the precise positioning and/or deprotonation of Y356 (Figure 7). Furthermore, this process must be reversible in order to account for our inability to observe any changes in the Y• concentration and for the V/K isotope effects on nucleotide reduction observed in the steady state (*41*, *42*). No V_{max} isotope effects for nucleotide reduction have been observed with either the class I or II RNRs using the normal substrate and wt enzyme (*41*, *54*). The conversion of NDP to dNDP is complex (chemistry, step 4), in which loss of water from the 2′-position of NDP is proposed to be irreversible, providing an important driving force for the overall reduction process (*55*). In addition, the rate-limiting step within the chemistry is proposed to be the reduction of the 3′-ketodeoxynucleotide intermediate (Scheme 1) via a disulfide radical anion (*56*). Kinetic modeling suggests that the chemistry (up to and including the first irreversible step) must occur with a rate constant of >500 s^{-1}, or changes in the concentration of Y• (our lower limit of detection is ~5% of the total Y•) would have been detected. The value of 500 s^{-1} is reasonable, given the rates of dNTP production of 20−50 s^{-1} measured for the structurally homologous class II RNR. In the chemical reaction catalyzed by both the class I and II RNRs, reduction of the 3′-ketodeoxynucleotide, but not 3′-carbon hydrogen bond cleavage, is thought to be the rate-limiting step in deoxynucleotide formation. For the class I enzyme, step 4 is followed by an irreversible PCET step, a process that is favored thermodynamically and would also involve amino acid radical intermediates. We have assigned a modest rate constant of $>10^3$ s^{-1} for this process as well. The irreversibility of step 5 is consistent with our inability to detect ^3H_2O when RNR was incubated with [3′-^{3}H]-dUDP of very high specific activity (*41*). Once dNDP has dissociated, oxidized RNR must reorganize itself so that it can catalyze additional rounds of nucleotide reduction. The details of this reduction remain to be elucidated, but likely involve the dissociation of R1 from R2, possible changes in the oligomeric state of R1, binding of R1 to reductant TR, and then reassociation with R2, substrate, and effector.

A number of previous experimental observations can be accommodated by this model (Figure 1). First we have previously shown that there are V/K isotope effects on the nucleotide reduction process (*41*, *42*). Using the ^{3}H and ^{2}H isotope effects measured with [3′-^{x}H]-UDP, one can calculate a ^Dk of 5, based on the Swain−Schaad relationship and the Northrop equation (*57*, *58*). While we have not yet attempted to measure the deuterium isotope effect on k_{obs} in the pre-steady state using [3′-^{2}H]-NDPs, it has been demonstrated that, using [3′-^{2}H]-UDP as substrate, no changes in the concentration of Y• is observed. Using the present kinetic model, slowing the chemistry down to 100 s^{-1} is insufficient to cause a detectable change in the Y•, in agreement with the experimental observations.

The model also provides an explanation for the unusual enzyme concentration dependence on dCDP formation (Figure 6), as first reported by Erickson (*30*). Studies with the class II RNR have previously demonstrated that the rate-limiting step is re-reduction of the enzyme (*7*), presumably the peripheral disulfide, as suggested by the rapid disulfide interchange observed by Erickson (*29*). Re-reduction, in the case of the class I RNRs, is much more complex due to the presence of the second subunit and the dimeric nature of R1 and R2. As the concentrations of the proteins (R1, R2, TR) are increased, one can readily rationalize why certain steps during re-reduction would be slowed. The complexity associated with re-reduction of R1 also explains the unusual fact that the specific activity of R1, measured in the presence of saturating R2, is always less than the specific activity of R2 in the presence of saturating R1. When R2 is assayed in the presence of excess R1, there are additional R1 molecules in the reduced state after the first dNDP formation, with which R2 can interact to generate additional dNDPs. Servicing a second R1, however, requires the re-formation of the Y• on R2. These data suggest that the tyrosine on R2 is reoxidized to Y• after each turnover. R1 in the presence of excess R2, on the other hand, must be re-converted into the reduced form for additional turnovers to occur, a process that is complex and can be partially rate-limiting depending on the protein concentrations. These results are strikingly similar to the class II RNR, where one AdoCbl can service multiple RNRs before the first RNR is re-reduced (*7*). The model presented in Figure 1 is useful as the starting point for designing experiments to study radical initiation and to understand the dynamics of protein interactions necessary for nucleotide reduction.

Finally, one perplexing observation from the pre-steady-state experiments remains to be explained. The stoichiometry of dCDP formation, observed with both wt R1 and C754/C759S R1 in the rapid single kinetic phase under pre-steady-state conditions, is greater than the amount of Y• per R2. The numbers of dCDPs (1.7 ± 0.4 and 1.6 ± 0.3 equiv, wt and mutant R1, respectively) support the model that both monomers of R1 are active. The present structural model of RNR as a symmetrical (1:1) complex between R1 and R2

(*25*, *27*) and the observation that the number of dCDPs is greater than the number of Y•s together demand that one Y• is able to access and initiate nucleotide reduction in each active site of the R1 dimer.

One possible model is that the Y• on one monomer of R2 can rapidly generate a Y• on the second monomer of R2, thereby catalyzing formation of two dCDPs, one in the active site of each monomer of R1, without dissociation of the R1R2 complex. However, Sjöberg et al have demonstrated, using a heterodimer of R2 in which one monomer has 30 amino acids removed from its C-terminus, that the Y• on one subunit cannot re-distribute to the second subunit, even in the presence of R1, substrate, and effector (*59*). The simplest interpretation of these results is that ET between Y122 of each monomer of R2 is unlikely. Nonetheless, one cannot exclude the possibility that the C-terminal tail missing in the construct, or more specifically, Y356 (Figure 7), plays an essential role in the generation of the Y• on the second monomer of R2.

A second possible model is that a single Y• per R2 dimer is capable of generating a S• in each monomer of R1 (R1 and R1′, Figure 7). This communication could occur through an alternative ET pathway, or through re-organization of R2 within an R1R2 complex. The ET between R1 and R2 most likely requires amino acid radical intermediates (*26*, *60*, *61*). Figure 7 shows the proposed pathway of communication between the monomers of R2 (R2 and R2′) and the monomers of R1 (R1 and R1′) (dashed line on the left, Figure 7). The ET pathway relies on a docking model for R1 and R2 proposed based on the shape complementarity of the structures (*25*) and many biochemical studies (*60*−*63*). Furthermore, comparison of ∼140 class I RNR sequences reveals that all of the conserved aromatic residues have been assigned roles in either catalysis (Y122 of R2), O_2 binding to R2 (F208 and F212 of R2), or the proposed long-range PCET pathway (W48 and Y356 of R2, Y730 and Y731 of R1) (*6*). The absence of conserved aromatic residues of unspecified function thus renders a previously undiscovered, alternative ET pathway highly unlikely. However, an ET pathway involving residues Y122 to W48 (monomer R2), to W48′ and Y356′ (monomer R2′), to Y731′, Y730′, and finally C439′ (monomer R1′) might be feasible (solid line, Figure 7). The distance between W48 of each R2 monomer is approximately 17 Å, a distance at which ET without conformational reorganization could be fast enough to account for the single-exponential phase of rapid product formation (*26*, *64*).

A subset of this model would be that R2 can reorganize with respect to the R1 monomers without complex dissociation. The structural complexity of this model and the kinetic requirement that the protein re-organization steps must be fast, however, make this model unattractive. At present, an alternative ET pathway that involves inter-monomer communication (solid line, Figure 7) represents the most viable, although not particularly appealing, model. Further studies are required to understand the structural basis for the interactions between R1 and R2, and the conformational dynamics of the complex.

Summary. Steady-state and pre-steady-state experiments on the *E. coli* class I RNR have provided new mechanistic insights into this class of RNRs. First, the rate determining step in the pre-steady state is a substrate/effector gated conformational change preceding rapid PCET, S• generation, and rapid nucleotide reduction. Second, comparison of kinetic data from the pre-steady-state and steady-state experiments at physiological concentrations of R1, R2, and thioredoxin suggest that, in the steady state, re-reduction of oxidized R1 becomes at least partially rate-limiting. Third, our data suggest that the Y• is reduced and reoxidized on each turnover. To formulate a detailed kinetic model now requires an understanding of the amount of Y• per R2 present *in vivo*, and the kinetic as well as the structural details for R1−R2 interactions fine-tuned by nucleotide substrates and deoxynucleotide effectors.

REFERENCES

1. Licht, S., and Stubbe, J. (1999) in *Comprehensive Natural Products Chemistry* (Barton, S. D., Nakanishi, K., Meth-Cohn, O., and Poulter, C. D., Eds.) pp 163, Elsevier Science, New York.
2. Jordan, A., and Reichard, P. (1998) Ribonucleotide reductases, *Annu. Rev. Biochem. 67*, 71−98.
3. Elledge, S. J., Zhou, Z., Allen, J. B., and Navas, T. A. (1993) DNA damage and cell cycle regulation of ribonucleotide reductase, *BioEssays 15*, 333−9.
4. Stubbe, J. (1998) Ribonucleotide reductases in the twenty-first century, *Proc. Natl. Acad. Sci. U.S.A. 95*, 2723−4.
5. Stubbe, J., and van der Donk, W. A. (1998) Protein radicals in enzyme catalysis, *Chem. Rev. 98*, 705−62.
6. Eklund, H., Uhlin, U., Farnegardh, M., Logan, D. T., and Nordlund, P. (2001) Structure and function of the radical enzyme ribonucleotide reductase, *Prog. Biophys. Mol. Biol. 77*, 177−268.
7. Licht, S. S., Lawrence, C. C., and Stubbe, J. (1999) Class II ribonucleotide reductases catalyze carbon−cobalt bond reformation on every turnover, *J. Am. Chem. Soc. 121*, 7463−8.
8. Licht, S. S., Booker, S., and Stubbe, J. (1999) Studies on the catalysis of carbon−cobalt bond homolysis by ribonucleoside triphosphate reductase: Evidence for concerted carbon−cobalt bond homolysis and thiyl radical formation, *Biochemistry 38*, 1221−33.
9. Licht, S. S., Lawrence, C. C., and Stubbe, J. (1999) Thermodynamic and kinetic studies on carbon−cobalt bond homolysis by ribonucleoside triphosphate reductase: The importance of entropy in catalysis, *Biochemistry 38*, 1234−42.
10. Licht, S., Gerfen, G. J., and Stubbe, J. (1996) Thiyl radicals in ribonucleotide reductases, *Science 271*, 477−81.
11. Orme-Johnson, W. H., Beinert, H., and Blakley, R. L. (1974) Cobamides and ribonucleotide reduction. XII. The electron paramagnetic resonance spectrum of "active coenzyme B12", *J. Biol. Chem. 249*, 2338−43.
12. Tamao, Y., and Blakley, R. L. (1973) Direct spectrophotometric observation of an intermediate formed from deoxyadenosylcobalamin in ribonucleotide reduction, *Biochemistry 12*, 24−34.
13. Thelander, L. (1973) Physicochemical characterization of ribonucleoside diphosphate reductase from *Escherichia coli*, *J. Biol. Chem. 248*, 4591−601.
14. Brown, N. C., and Reichard, P. (1969) Ribonucleoside diphosphate reductase. Formation of active and inactive complexes of proteins B1 and B2, *J. Mol. Biol. 46*, 25−38.
15. Lin, A. N., Ashley, G. W., and Stubbe, J. (1987) Location of the redox-active thiols of ribonucleotide reductase: Sequence similarity between the *Escherichia coli* and *Lactobacillus leichmannii* enzymes, *Biochemistry 26*, 6905−9.
16. Mao, S. S., Johnston, M. I., Bollinger, J. M., and Stubbe, J. (1989) Mechanism-based inhibition of a mutant *Escherichia coli* ribonucleotide reductase (cysteine-225→serine) by its substrate CDP, *Proc. Natl. Acad. Sci. U.S.A. 86*, 1485−9.
17. Mao, S. S., Holler, T. P., Bollinger, J. M., Jr., Yu, G. X., Johnston, M. I., and Stubbe, J. (1992) Interaction of C225SR1 mutant subunit of ribonucleotide reductase with R2 and nucleoside diphosphates: Tales of a suicidal enzyme, *Biochemistry 31*, 9744−51.
18. Mao, S. S., Holler, T. P., Yu, G. X., Bollinger, J. M., Jr., Booker, S., Johnston, M. I., and Stubbe, J. (1992) A model for the role of multiple cysteine residues involved in ribonucleotide reduction: Amazing and still confusing, *Biochemistry 31*, 9733−43.

19. Mao, S. S., Yu, G. X., Chalfoun, D., and Stubbe, J. (1992) Characterization of C439SR1, a mutant of *Escherichia coli* ribonucleotide diphosphate reductase: Evidence that C439 is a residue essential for nucleotide reduction and C439SR1 is a protein possessing novel thioredoxin-like activity, *Biochemistry 31*, 9752−9.
20. Åberg, A., Hahne, S., Karlsson, M., Larsson, A., Ormö, M., Ahgren, A., and Sjöberg, B.-M. (1989) Evidence for two different classes of redox-active cysteines in ribonucleotide reductase of *Escherichia coli*, *J. Biol. Chem. 264*, 12249−52.
21. Kashlan, O. B., and Cooperman, B. S. (2003) Comprehensive model for allosteric regulation of mammalian ribonucleotide reductase: Refinements and consequences, *Biochemistry 42*, 1696−706.
22. Kashlan, O. B., Scott, C. P., Lear, J. D., and Cooperman, B. S. (2002) A comprehensive model for the allosteric regulation of mammalian ribonucleotide reductase. Functional consequences of ATP- and dATP-induced oligomerization of the large subunit, *Biochemistry 41*, 462−74.
23. Brown, N. C., and Reichard, P. (1969) Role of effector binding in allosteric control of ribonucleoside diphosphate reductase, *J. Mol. Biol. 46*, 39−55.
24. Thelander, L., and Reichard, P. (1979) Reduction of ribonucleotides, *Annu. Rev. Biochem. 48*, 133−58.
25. Uhlin, U., and Eklund, H. (1994) Structure of ribonucleotide reductase protein R1, *Nature 370*, 533−9.
26. Stubbe, J., Nocera, D. G., Yee, C. S., and Chang, M. C. Y. (2003) Radical initiation in the class I ribonucleotide reductase: Long-range proton coupled electron transfer? *Chem. Rev.*, in press.
27. Nordlund, P., Sjöberg, B.-M., and Eklund, H. (1990) Three-dimensional structure of the free radical protein of ribonucleotide reductase, *Nature 345*, 593−8.
28. Nordlund, P., and Eklund, H. (1993) Structure and function of the *Escherichia coli* ribonucleotide reductase protein R2, *J. Mol. Biol. 232*, 123−64.
29. Erickson, H. K. (2001) Kinetics in the pre-steady state of the formation of cystines in ribonucleoside diphosphate reductase: Evidence for an asymmetric complex, *Biochemistry 40*, 9631−7.
30. Erickson, H. K. (2000) Formation of the cystine between cysteine 225 and cysteine 462 from ribonucleoside diphosphate reductase is kinetically competent, *Biochemistry 39*, 9241−50.
31. Lunn, C. A., Kathju, S., Wallace, C., Kushner, S., and Pigiet, V. (1984) Amplification and purification of plasmid-encoded thioredoxin from Escherichia coli K12, *J. Biol. Chem. 259*, 10469−74.
32. Chivers, P. T., Prehoda, K. E., Volkman, B. F., Kim, B. M., Markley, J. L., and Raines, R. T. (1997) Microscopic pK_a values of *Escherichia coli* thioredoxin, *Biochemistry 36*, 14985−91.
33. Russel, M., and Model, P. (1985) Direct cloning of the *trx* gene that encodes thioredoxin reductase, *J. Bacteriol. 163*, 238−42.
34. Salowe, S., Bollinger, J. M., Jr., Ator, M., Stubbe, J., McCraken, J., Peisach, J., Samano, M. C., and Robins, M. J. (1993) Alternative model for mechanism-based inhibition of *Escherichia coli* ribonucleotide reductase by 2′-azido-2′-deoxyuridine 5′-diphosphate, *Biochemistry 32*, 12749−60.
35. Thelander, L., Sjöberg, B. R., and Eriksson, S. (1978) Ribonucleoside diphosphate reductase (*Escherichia coli*), *Methods Enzymol. 51*, 227−37.
36. Salowe, S. P., and Stubbe, J. (1986) Cloning, overproduction, and purification of the B2 subunit of ribonucleoside-diphosphate reductase, *J. Bacteriol. 165*, 363−6.
37. Usova, E. V., and Eriksson, S. (1997) The effects of high salt concentrations on the regulation of the substrate specificity of human recombinant deoxycytidine kinase, *Eur. J. Biochem. 248*, 763−6.
38. Bollinger, J. M., Jr., Tong, W. H., Ravi, N., Huynh, B. H., Edmondson, D. E., and Stubbe, J. A. (1995) Use of rapid kinetics methods to study the assembly of the diferric-tyrosyl radical cofactor of *E. coli* ribonucleotide reductase, *Methods Enzymol. 258*, 278−303.
39. Steeper, J. R., and Steuart, C. D. (1970) A rapid assay for CDP reductase activity in mammalian cell extracts, *Anal. Biochem. 34*, 123−30.
40. Kuzmic, P. (1996) Program DYNAFIT for the analysis of enzyme kinetic data: Application to HIV proteinase, *Anal. Biochem. 237*, 260−73.
41. Stubbe, J., Ator, M., and Krenitsky, T. (1983) Mechanism of ribonucleoside diphosphate reductase from *Escherichia coli*. Evidence for 3′ C-H bond cleavage, *J. Biol. Chem. 258*, 1625−31.
42. Stubbe, J., and Ackles, D. (1980) On the mechanism of ribonucleoside diphosphate reductase from *Escherichia coli*. Evidence for 3′ C−H bond cleavage, *J. Biol. Chem. 255*, 8027−30.
43. Thelander, L. (1974) Reaction mechanism of ribonucleoside diphosphate reductase from *Escherichia coli*. Oxidation-reduction-active disulfides in the B1 subunit, *J. Biol. Chem. 249*, 4858−62.
44. Sintchak, M. D., Arjara, G., Kellogg, B. A., Stubbe, J., and Drennan, C. L. (2002) The crystal structure of class II ribonucleotide reductase reveals how an allosterically regulated monomer mimics a dimer, *Nat. Struct. Biol. 9*, 293−300.
45. Booker, S., Licht, S., Broderick, J., and Stubbe, J. (1994) Coenzyme B12-dependent ribonucleotide reductase: Evidence for the participation of five cysteine residues in ribonucleotide reduction, *Biochemistry 33*, 12676−85.
46. Climent, I., Sjöberg, B.-M., and Huang, C. Y. (1991) Carboxyl-terminal peptides as probes for *Escherichia coli* ribonucleotide reductase subunit interaction: Kinetic analysis of inhibition studies, *Biochemistry 30*, 5164−71.
47. Climent, I., Sjöberg, B.-M., and Huang, C. Y. (1992) Site-directed mutagenesis and deletion of the carboxyl terminus of *Escherichia coli* ribonucleotide reductase protein R2. Effects on catalytic activity and subunit interaction, *Biochemistry 31*, 4801−7.
48. Scott, C. P., Kashlan, O. B., Lear, J. D., and Cooperman, B. S. (2001) A quantitative model for allosteric control of purine reduction by murine ribonucleotide reductase, *Biochemistry 40*, 1651−61.
49. Allard, P., Kuprin, S., Shen, B., and Ehrenberg, A. (1992) Binding of the competitive inhibitor dCDP to ribonucleoside-diphosphate reductase from Escherichia coli studied by 1H NMR. Different properties of the large protein subunit and the holoenzyme, *Eur. J. Biochem. 208*, 635−42.
50. Shen, B., Allard, P., Kuprin, S., and Ehrenberg, A. (1992) Studies on ribonucleoside-diphosphate reductase from Escherichia coli. The product dCDP is a competitive inhibitor and functions as a spectroscopic probe for the substrate binding site; demonstration by enzyme kinetics and ^{1}H NMR, *Eur. J. Biochem. 208*, 631−4.
51. Ormö, M., and Sjöberg, B.-M. (1990) An ultrafiltration assay for nucleotide binding to ribonucleotide reductase, *Anal. Biochem. 189*, 138−41.
52. Soderman, K., and Reichard, P. (1986) A nitrocellulose filter binding assay for ribonucleotide reductase, *Anal. Biochem. 152*, 89−93.
53. von Dobeln, U., and Reichard, P. (1976) Binding of substrates to Escherichia coli ribonucleotide reductase, *J. Biol. Chem. 251*, 3616−22.
54. Ashley, G. W., Harris, G., and Stubbe, J. (1986) The mechanism of Lactobacillus leichmannii ribonucleotide reductase. Evidence for 3′ carbon−hydrogen bond cleavage and a unique role for coenzyme B12, *J. Biol. Chem. 261*, 3958−64.
55. Lenz, R., and Giese, B. (1997) Studies on the mechanism of ribonucleotide reductases, *J. Am. Chem. Soc. 119*, 2784−94.
56. Lawrence, C. C., Bennati, M., Obias, H. V., Bar, G., Griffin, R. G., and Stubbe, J. (1999) High-field EPR detection of a disulfide radical anion in the reduction of cytidine 5′-diphosphate by the E441Q R1 mutant of Escherichia *coli* ribonucleotide reductase, *Proc. Natl. Acad. Sci. U.S.A. 96*, 8979−84.
57. Northrop, D. B. (1982) Deuterium and tritium kinetic isotope effects on initial rates, *Methods Enzymol. 87*, 607−25.
58. Swain, C. G., Stivers, E. C., Reuwer, J., Joseph F., and Schaad, L. J. (1958) Use of hydrogen isotope effects to identify the attacking nucleophile in the enolization of ketones catalyzed by acetic acid, *J. Am. Chem. Soc. 80*, 5885−93.
59. Sjöberg, B.-M., Karlsson, M., and Jörnvall, H. (1987) Half-site reactivity of the tyrosyl radical of ribonucleotide reductase from *Escherichia coli*, *J. Biol. Chem. 262*, 9736−43.
60. Ekberg, M., Sahlin, M., Eriksson, M., and Sjöberg, B.-M. (1996) Two conserved tyrosine residues in protein R1 participate in an intermolecular electron transfer in ribonucleotide reductase, *J. Biol. Chem. 271*, 20655−9.
61. Ekberg, M., Pötsch, S., Sandin, E., Thunnissen, M., Nordlund, P., Sahlin, M., and Sjöberg, B.-M. (1998) Preserved catalytic activity in an engineered ribonucleotide reductase R2 protein with a nonphysiological radical transfer pathway—the importance of hydrogen bond connections between the participating residues, *J. Biol. Chem. 273*, 21003−8.

62. Rova, U., Adrait, A., Pötsch, S., Gräslund, A., and Thelander, L. (1999) Evidence by mutagenesis that Tyr(370) of the mouse ribonucleotide reductase R2 protein is the connecting link in the intersubunit radical transfer pathway. *J. Biol. Chem. 274*, 23746−51.
63. Rova, U., Goodtzova, K., Ingemarson, R., Behravan, G., Gräslund, A., and Thelander, L. (1995) Evidence by site-directed mutagenesis supports long-range electron transfer in mouse ribonucleotide reductase, *Biochemistry 34*, 4267−75.
64. Gray, H. B., and Winkler, J. R. (1997) Electron tunneling in structurally engineered proteins, *J. Electroanal. Chem. 438*, 43−7.
65. Barshop, B. A., Wrenn, R. F., and Frieden, C. (1983) Analysis of numerical methods for computer simulation of kinetic processes: Development of KINSIM−a flexible, portable system, *Anal. Biochem. 130*, 134−45.

BI034374R